ChemComm

Check for updates

Molecular layer deposition of Li-ion conducting "Lithicone" solid electrolytes†

Eric Kazyak, [ID] ‡[a] Minjeong Shin,‡[a] William S. LePage,[a] Tae H. Cho[a] and Neil P. Dasgupta [ID] ⋆[ab]

We demonstrate the fabrication of Li-containing ("lithicone") thin films prepared *via* molecular layer deposition (MLD) using lithium *tert*-butoxide and ethylene glycol. X-ray photoelectron spectroscopy reveals that the stoichiometry of the lithicone is $Li_{1.5}C_2O_{1.8}$ (H omitted), with C−O−Li moieties present in the film. The bonding environment of lithicone is distinct from that of lithium carbonate or MLD alucone films. Electrochemical impedance spectroscopy measurements show that annealed lithicone films exhibit room temperature ionic conductivity of $3.6\text{–}5 \times 10^{-8}$ S cm^{-1} with an activation energy of $\sim$0.6 eV. The lithicone MLD process provides a pathway to further develop hybrid inorganic−organic Li-ion conducting materials for future battery applications.

Atomic layer deposition (ALD), and its organic analog molecular layer deposition (MLD), are gas-phase thin film deposition techniques that have been broadly applied in lithium battery applications.[1,2] This includes interfacial coatings for anodes and cathodes, deposition of electrodes and solid electrolytes, and fabrication of thin-film/three-dimensional batteries.[3–6] ALD/MLD are based on self-limiting surface reactions where gaseous precursors are sequentially exposed to the substrate to grow a film in a layer-by-layer manner.[1,2] The unique capability of ALD/MLD to conformally coat non-planar geometries with precise control of thickness and composition enables the formation of passivation layers that can prevent electrode materials from degradation at low/high electrochemical potentials, while facilitating the flux of ions across interfaces.[3–8]

Among the various ALD/MLD films developed for battery applications, Li-ion conducting films are receiving great interest due to their potential to be directly adopted as solid electrolytes or interlayer materials that allow ion transport through the film

without significantly increasing cell impedance.[9] In the past decade, significant advancements have been made in developing Li-ion conducting ALD materials.[10–20] Several Li-ion conducting ALD films such as Li_xAl_yO, Li_xAl_yS, $LiTa_xO_y$, LiPON, $Li_7La_3Zr_2O_{12}$, and Li_3BO_3–Li_2CO_3 have been reported with ionic conductivities ranging $10^{-10}\text{–}10^{-6}$ S cm^{-1}.[10–20] Despite great achievements in fabricating ALD thin films for Li-based batteries, research efforts to develop Li-conducting films prepared *via* MLD have been limited.

MLD is an organic equivalent to ALD where organic precursors are employed as oxidizers. Similar to ALD, MLD is characterized by sequential and self-limiting surface reactions that result in a conformal and uniform coating of polymeric or inorganic–organic hybrid thin films ("metalcones").[2] MLD films have been explored for battery applications where increased mechanical ductility of the coating is desirable, such as surface coatings for high volume expansion electrode materials (*e.g.* Si anodes) or as an interlayer in solid-state batteries.[4,5,21–23]

In liquid electrolyte systems, Piper *et al.* investigated the MLD coating of alucone (deposited using trimethylaluminum and glycerol precursors) as a buffer layer for Si anodes.[22] Si nanoparticles coated with alucone exhibit superior cycling stability relative to bare Si nanoparticles, which is attributed to the formation of a stable passivation layer that is able to accommodate large volume changes of the active material.[22] In another work, Sun and co-workers demonstrated the use of dual protective layer of ALD Al_2O_3 as the inner layer and MLD alucone as the outer layer to stabilize the Li metal anode, showing enhanced cycling stability and suppressed growth of mossy Li.[21] In solid-state batteries, alucone was shown to be more effective than ALD Al_2O_3 as an interlayer between Li metal and $Li_{10}SnP_2S_{12}$ solid electrolyte, which was attributed to the improved mechanical properties of the MLD film.[23]

Despite these demonstrations of MLD interlayers in battery applications, alucone films do not contain lithium as-deposited, and instead, rely on chemical and/or electrochemical lithiation of the films during cycling. This leads to a general lack of control over the ionic conductivity of the films, which is also difficult to

[a] Department of Mechanical Engineering, University of Michigan, Ann Arbor, MI 48109, USA. E-mail: ndasgupt@umich.edu

[b] Department of Materials Science & Engineering, University of Michigan, Ann Arbor, MI 48109, USA

‡ These authors contributed equally to this work.

measure, and may evolve during extended cycling. Therefore, there is a need to develop Li-containing MLD films that act as solid electrolytes with high ionic conductivity, which could be used in a wide range of battery applications. However, there are only a few Li-containing MLD films reported to date, and no reported measurements of the ionic conductivity values of MLD films.[24–27]

In this work, MLD was used to deposit Li-containing organic thin films that we refer to as ''lithicone'', in analogy with other metalcone films.[2] Lithium *tert*-butoxide (LiO^{t}Bu) was used as the lithium precursor and ethylene glycol (EG) was used as the organic linker. This specific combination of precursors has not been previously reported. Spectroscopic ellipsometry, *in situ* quartz crystal microbalance (QCM), and atomic force microscopy (AFM) measurements were performed to study the MLD growth characteristics. The lithicone film composition and chemical environment was characterized using X-ray photoelectron spectroscopy (XPS). The room temperature Li-ion conductivity of the annealed lithicone film is $3.6–5 \times 10^{-8}$ S cm^{-1}, measured by electrochemical impedance spectroscopy (EIS), which illustrates the potential of these films as solid electrolyte layers.

For the choice of lithium precursor, LiO^{t}Bu was selected because it has been successfully demonstrated in other Li-containing ALD films, owing to a sufficiently high vapor pressure and demonstration of self-limiting surface reactions.[10,12–18] EG was used as the organic precursor, owing to its high vapor pressure and thermal stability within the deposition temperature window.[2,28] A saturation study of the lithicone MLD process was performed by varying precursor pulse length of both the LiO^{t}Bu and EG precursors (Fig. 1a, b and Fig. S1, ESI†). The thicknesses of the lithicone films after 200 MLD cycles were measured by spectroscopic ellipsometry. As shown in Fig. 1a and b, the film thickness increases with increasing precursor exposure time before reaching a plateau, which indicates the self-limiting nature of this MLD process. Pulse saturation time was determined to be 8 s for LiO^{t}Bu and 0.15 s for EG.

The measured thicknesses of the films as a function of MLD cycle number is shown in Fig. 1c. The film thickness increases linearly with increasing cycle number, corresponding to the growth-per-cycle (GPC) of 2.6 Å cycle^{-1}. We note that the linear regression line does not pass through origin, suggesting the presence of initial nucleation delay in the initial cycles on a Si substrate. A similar growth profile with a nucleation delay was reported in a previous MLD study using LiO^{t}Bu and 1,3-propanediol.[26] We performed AFM measurements to further study the initial film nucleation, which will be discussed below.

In situ QCM studies were performed to monitor the mass uptake during film growth. Fig. S2 (ESI†) shows that the mass uptake increases linearly, which is in good agreement with the trend shown in Fig. 1c. Fig. 1d shows a magnified view of 3 representative cycles from a longer deposition. As shown, the LiO^{t}Bu pulse results in an initial mass gain followed by a gradual decrease. A similar trend is observed after the EG exposure. The slight decrease in mass during purging is attributed to the initial adsorption/absorption of precursor onto the surface and into the bulk, followed by desorption.[28,29]
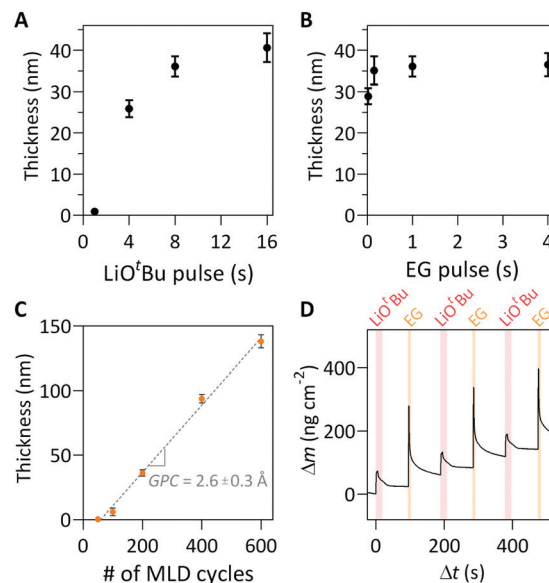

Fig. 1 Thickness of the lithicone film after 200 cycles as a function of (a) LiO^{t}Bu and (b) EG pulse lengths, showing self-limiting growth characteristics. (c) The film thickness as a function of number of MLD cycle numbers, showing linear growth. Error bars in panels (a–c) represent film uniformity across a 100 mm-diameter wafer. (d) *In situ* QCM measured during sequential exposure of LiO^{t}Bu and EG. The shaded color regions represent LiO^{t}Bu and EG pulses, respectively. The film deposition temperature was 135 °C in all cases.

The saturation-limited growth characteristics were further investigated by depositing the film on a Si trenches (Fig. S3, ESI†). The SEM images show conformal deposition of the lithicone film on Si microstructures, demonstrating the non-line-of-sight deposition characteristics of the MLD process.

We performed AFM analysis to study the morphology and growth characteristics of lithicone as a function of cycle number. As shown in Fig. 2, the surface morphology of the film evolves with cycle number, along with the RMS roughness. During the initial deposition cycles, the film morphology consists of small grains, which grow vertically and laterally with increasing cycle number. This evolution corresponds well with the increase of RMS roughness between cycles 50–150. This is consistent with the nucleation delay observed in ellipsometry measurement shown in Fig. 1c. After 150 cycles, the film morphology remains relatively unchanged, and the RMS roughness value reaches a plateau. This result implies that once the initial nucleation stage is complete, the film grows in a layer-by-layer manner.

XPS was performed to determine the composition and chemical environment of the lithicone film (Fig. 3). Fig. 3 shows XPS O 1s, C 1s, and Li 1s core scans of the lithicone film deposited at 135 °C. For reference, XPS spectra of alucone (MLD of TMA + EG) and lithium carbonate (ALD of LiO^{t}Bu + H$_2$O + CO$_2$) are also shown in the first and second rows of Fig. 3, respectively. Curve fitting of the XPS spectra was performed to deconvolute each species. Peak assignments are based on previous values reported in the literature along with known standard samples.[26,28,30–32]
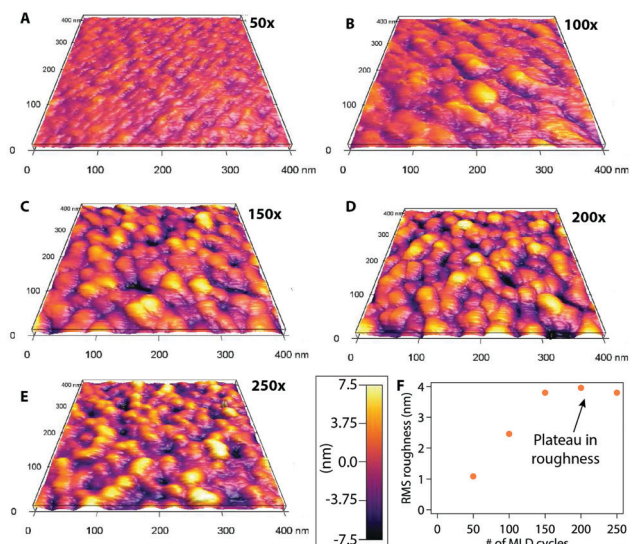
Fig. 2 AFM images of lithicone films at (a) 50, (b) 100, (c) 150, (d) 200, (e) 250 deposition cycles. (f) RMS roughness as a function of MLD cycle number is shown.
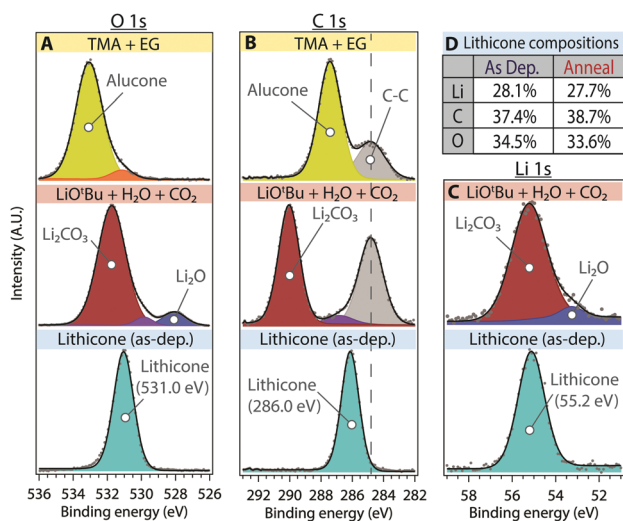

Fig. 3 XPS spectra of the alucone (first row), lithium carbonate (second row), as-deposited lithicone film (third row). Core scans (A) O 1s, (B) C 1s, and (C) Li 1s are shown. XPS peak assignments are as follows: C–O in alucone (yellow), adventitious carbon (grey), Li_2CO_3 (red), Li_2O (dark blue), C–O–Li in lithicone (light blue). (D) Atomic compositions of the as-deposited and annealed lithicone film are tabulated.

As shown in Fig. 3d, the prepared lithicone film contains ∼28 atomic % of lithium, demonstrating successful incorporation of lithium into the MLD film. The stoichiometry of the as-deposited lithicone film was calculated to be $Li_{1.5}C_2O_{1.8}$ (hydrogen content not included).

As shown in Fig. 3, the XPS spectra of alucone can be fit with a primary peak corresponding to C–O bonding – 533.1 eV for the O 1s peak and 287.4 eV for C 1s peak (yellow). The lithicone film exhibits a distinct chemical environment from that of alucone, showing predominant peaks at 531.0 eV for O 1s, 286.0 eV for C 1s, and 55.2 eV for Li 1s (light blue), associated with C–O–Li moieties (Fig. 3). The binding energy of the primary peak in lithicone is significantly lower than that of alucone, for both the O 1s and C 1s peaks. This is the consequence of Li association with C–O bonds, forming C–O–Li bonding environments in lithicone.

Next, we examine the ionic conductivity of lithicone to evaluate the possibility of using lithicone in Li battery applications. The ionic conductivity was measured by depositing the film onto interdigitated Pt electrodes (Fig. S4, ESI†), as reported previously.[13,17,18] This electrode geometry enables characterization of the ionic and electronic conduction properties of thin films without the need to further deposit blocking electrodes on top of the film after the ALD/MLD process. Electrochemical impedance spectroscopy (EIS) was conducted on a lithicone film deposited on Pt electrode. The ionic conductivity of the as-deposited lithicone was unmeasurable. After post-deposition annealing at 350 °C, the film exhibits an irreversible increase in ionic conductivity upon heating and subsequent cooling back to 30 °C. This is similar to the behavior observed for ALD of Li_3BO_3–Li_2CO_3, where the increase in ionic conductivity is attributed to structural changes in the film.[18] The impact of annealing temperature on ionic conductivity and transference number is shown in Fig. S5 (ESI†).

We performed XPS analysis on the lithicone film after annealing, and observed subtle changes to the core spectra (Fig. S6, ESI†), and negligible changes to the overall composition. X-ray diffraction (XRD) analysis show that the lithicone film remains amorphous after annealing, suggesting no phase transition upon annealing (Fig. S7, ESI†). Fourier-transform infrared spectroscopy (FTIR) spectra of the as-deposited and annealed film show that the chemical bonding of the film remains unchanged with annealing, consistent with the XPS analysis (Fig. S8, ESI†). A full mechanistic understanding of conductivity increase with annealing will be the subject of future studies.

Representative Nyquist plots of films after post-deposition annealing were collected at several temperatures are shown in Fig. 4a. The Nyquist plots were fit with the equivalent circuit shown in the inset of Fig. 4a to quantify the resistance of each cell component. The linear relationship of the $ln(\sigma T)$ vs. T^{-1} data allows for determination of the activation energy, as shown in Fig. 4b.

Our measurement shows that the annealed lithicone film deposited at 175 °C exhibits an ionic conductivity of 3.6×10^{-8} S cm^{-1} at 30 °C with activation energy of 0.6 eV. The lithicone film deposited at 135 °C shows similar ionic conductivity trend, with a value of 5×10^{-8} S cm^{-1} at 30 °C (Fig. S9, ESI†). To the best of our knowledge, this is the first reported Li-ion conductivity of an MLD film. The ionic conductivity and activation energy value are comparable to several Li-ion conducting thin films prepared by ALD such as $LiAlO_2$, LiPON, Li_xAl_yS, $LiAlF_4$, and $LiNb_xO_y$.[11,13–16] Although the film exhibits relatively low ionic conductivity compared to bulk solid electrolytes, the additional ohmic resistance introduced by a nanoscale thin film lithicone would be minimal. For example, a 10 nm thick
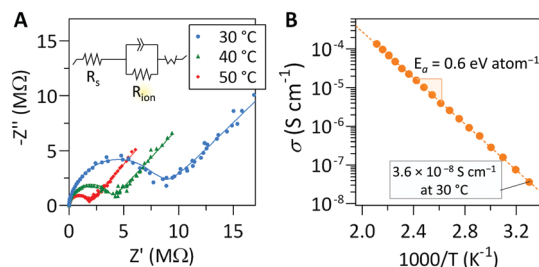
Fig. 4 Ionic conductivity measurement of the lithicone film obtained using interdigitated Pt electrode. (a) Nyquist plot measured at various temperatures with inset showing the equivalent circuit used to extract the resistance. The symbols represent the data and fit results are overlaid in solid line. (b) Arrhenius plot of conductivities of lithicone along with corresponding activation energy.

lithicone film corresponds to an area specific resistance of $\sim$28 Ω cm^2, which is lower than the interfacial impedance of many solid-state battery systems.

To confirm that the origin of conductivity is predominantly ionic, the electronic conductivity of the lithicone film was measured by chronoamperometry, and the corresponding Arrhenius plot is shown in Fig. S10 (ESI†). The measured electronic conductivity of the film is 5 to 6 orders-of-magnitude lower than the ionic conductivity, exhibiting an ionic transference number greater than 99.999%. Therefore, these films have the potential for use as either an interlayer or a bulk solid electrolyte in thin film batteries.

In summary, we have successfully deposited Li-containing organic thin films through a MLD process using LiO^{t}Bu and EG as precursors. The self-limiting surface reactions and film growth profiles were confirmed using spectroscopic ellipsometry and by monitoring mass gain by *in situ* QCM. We demonstrate that the lithicone film grows in a layer-by-layer manner showing surface saturation and linear increase in film thickness. The growth rate of film was 2.6 Å cycle^{-1} at a deposition temperature of 135 °C. XPS revealed the composition and chemical structure of the deposited lithicone film, with a bonding environment that is distinct from lithium carbonate or alucone. The films exhibit an ionic conductivity of 3.6 $\times$ 10^{-8} S cm^{-1} at 30 °C with an activation energy of 0.6 eV. This is the first quantified measurement of Li-ion conductivity in an MLD thin film to-date. This study will serve as a springboard to develop advanced organic/inorganic hybrid thin films for use in future battery applications. Further studies will focus on developing other Li-containing MLD processes using other precursors of varying functionalities and compositions.

Conflicts of interest

There are no conflicts to declare.

Notes and references

1 S. M. George, *Chem. Rev.*, 2010, **110**, 111–131.
2 S. M. George, A. A. Dameron and B. Yoon, *Acc. Chem. Res.*, 2009, **42**, 498–508.
3 X. Meng, X. Q. Yang and X. Sun, *Adv. Mater.*, 2012, **24**, 3589–3615.
4 C. Ban and S. M. George, *Adv. Mater. Interfaces*, 2016, **3**, 1600762.
5 Y. Zhao and X. Sun, *ACS Energy Lett.*, 2018, **3**, 899–914.
6 X. Wang and G. Yushin, *Energy Environ. Sci.*, 2015, **8**, 1889–1904.
7 L. Ma, R. B. Nuwayhid, T. Wu, Y. Lei, K. Amine and J. Lu, *Adv. Mater. Interfaces*, 2016, **3**, 1600564.
8 A. L. Davis, R. Garcia-Mendez, K. N. Wood, E. Kazyak, K.-H. Chen, G. Teeter, J. Sakamoto and N. P. Dasgupta, *J. Mater. Chem. A*, 2020, **12**, 6291–6302.
9 X. Meng, *Energy Storage Mater.*, 2020, **30**, 296–328.
10 J. Liu, M. N. Banis, X. Li, A. Lushington, M. Cai, R. Li, T. K. Sham and X. Sun, *J. Phys. Chem. C*, 2013, **117**, 20260–20267.
11 M. Nisula, Y. Shindo, H. Koga and M. Karppinen, *Chem. Mater.*, 2015, **27**, 6987–6993.
12 A. C. Kozen, A. J. Pearse, C. F. Lin, M. Noked and G. W. Rubloff, *Chem. Mater.*, 2015, **27**, 5324–5331.
13 Y. Cao, X. Meng and J. W. Elam, *ChemElectroChem*, 2016, **3**, 858–863.
14 J. Xie, A. D. Sendek, E. D. Cubuk, X. Zhang, Z. Lu, Y. Gong, T. Wu, F. Shi, W. Liu, E. J. Reed and Y. Cui, *ACS Nano*, 2017, **11**, 7019–7027.
15 B. Wang, Y. Zhao, M. N. Banis, Q. Sun, K. R. Adair, R. Li, T. K. Sham and X. Sun, *ACS Appl. Mater. Interfaces*, 2018, **10**, 1654–1661.
16 J. S. Park, X. Meng, J. W. Elam, S. Hao, C. Wolverton, C. Kim and J. Cabana, *Chem. Mater.*, 2014, **26**, 3128–3134.
17 E. Kazyak, K. H. Chen, K. N. Wood, A. L. Davis, T. Thompson, A. R. Bielinski, A. J. Sanchez, X. Wang, C. Wang, J. Sakamoto and N. P. Dasgupta, *Chem. Mater.*, 2017, **29**, 3785–3792.
18 E. Kazyak, K. H. Chen, A. L. Davis, S. Yu, A. J. Sanchez, J. Lasso, A. R. Bielinski, T. Thompson, J. Sakamoto, D. J. Siegel and N. P. Dasgupta, *J. Mater. Chem. A*, 2018, **6**, 19425–19437.
19 Y. Hu, A. Ruud, V. Miikkulainen, T. Norby, O. Nilsen and H. Fjellvåg, *RSC Adv.*, 2016, **6**, 60479–60486.
20 M. Putkonen, T. Aaltonen, M. Alnes, T. Sajavaara, O. Nilsen and H. Fjellvåg, *J. Mater. Chem.*, 2009, **19**, 8767–8771.
21 Y. Zhao, M. Amirmaleki, Q. Sun, C. Zhao, A. Codirenzi, L. V. Goncharova, C. Wang, K. Adair, X. Li, X. Yang, F. Zhao, R. Li, T. Filleter, M. Cai and X. Sun, *Matter*, 2019, **1**, 1215–1231.
22 D. M. Piper, J. J. Travis, M. Young, S. B. Son, S. C. Kim, K. H. Oh, S. M. George, C. Ban and S. H. Lee, *Adv. Mater.*, 2014, **26**, 1596–1601.
23 C. Wang, Y. Zhao, Q. Sun, X. Li, Y. Liu, J. Liang, X. Li, R. Lin, R. Li, K. R. Adair, L. Zhang, R. Yang, S. Lu and X. Sun, *Nano Energy*, 2018, **53**, 168–174.
24 M. Nisula and M. Karppinen, *Nano Lett.*, 2016, **16**, 1276–1281.
25 M. Nisula, J. Linnera, A. J. Karttunen and M. Karppinen, *Chem. – Eur. J.*, 2017, **23**, 2988–2992.
26 H. Wang, K. E. Gregorczyk, S. B. Lee, G. W. Rubloff and C. Lin, *J. Phys. Chem. C*, 2020, **124**, 6830–6837.
27 J. Heiska, M. Madadi and M. Karppinen, *Nanoscale Adv.*, 2020, **2**, 2441–2447.
28 A. A. Dameron, D. Seghete, B. B. Burton, S. D. Davidson, A. S. Cavanagh, J. A. Bertrand and S. M. George, *Chem. Mater.*, 2008, **20**, 3315–3326.
29 C. A. Wilson, R. K. Grubbs and S. M. George, *Chem. Mater.*, 2005, **17**, 5625–5634.
30 I. Ismail, A. Noda, A. Nishimoto and M. Watanabe, *Electrochim. Acta*, 2001, **46**, 1595–1603.
31 K. N. Wood and G. Teeter, *ACS Appl. Energy Mater.*, 2018, **1**, 4493–4504.
32 S. Jiao, X. Ren, R. Cao, M. H. Engelhard, Y. Liu, D. Hu, D. Mei, J. Zheng, W. Zhao, Q. Li, N. Liu, B. D. Adams, C. Ma, J. Liu, J. G. Zhang and W. Xu, *Nat. Energy*, 2018, **3**, 739–746.